MgB_2 thin-film bolometer for applications in far-infrared instruments on future planetary missions

B. Lakew[1], S. Aslam[1*], J. Brasunas[1], N. Cao[2, 3], N. Costen[2, 3], A. La[2], L. Nyguyen[2],

T. Stevenson[2], A. Waczynski[2]

[1] *NASA/Goddard Space Flight Center, Planetary Systems Laboratory, Code 693, Greenbelt, MD 20771, USA*

[2] *NASA/Goddard Space Flight Center, Detector Systems Branch, Code 553, Greenbelt, MD 20771, USA*

[3] *MEI Technologies Inc., 2525 Bay Area Blvd., Houston, TX 77058, USA*

Abstract

A SiN membrane based MgB_2 thin-film bolometer, with a non-optimized absorber, has been fabricated that shows an electrical noise equivalent power of 256 fW/√Hz operating at 30 Hz in the 8.5 -12.35 μm spectral bandpass. This value corresponds to an electrical specific detectivity of 7.6×10^{10} cm√Hz/W. The bolometer shows a measured blackbody (optical) specific detectivity of 8.8×10^{9} cm√Hz/W, with a responsivity of 701.5 kV/W and a first-order time constant of 5.2 ms. It is predicted that with the inclusion of a gold black absorber that a blackbody specific detectivity of 6.4×10^{10} cm/√Hz/W at an operational frequency of 10 Hz, can be realized for integration into future planetary exploration instrumentation where high sensitivity is required in the 17 - 250 μm spectral wavelength range.

PACS: 74.78.Bz High-T_c films; 95.85.Gn

Keywords: MgB_2 thin film; Bolometer; Thermal Detector; D^*

1. Introduction

* corresponding author: e-mail: shahid.aslam-1@nasa.gov

The superconducting critical temperature ($T_c = 39\text{K}$) of the simple binary, intermetallic MgB_2 [1] makes it a very good candidate for the development of the next generation of electro-optical devices (e.g. [2] [3] [4] [5] [6]). In particular, recent advances in deposition techniques to attain high quality polycrystalline MgB_2 thin-film deposited on SiN-Si substrates, with $T_c \approx 38\text{K}$ [7] [8] [9] together with the observed low voltage noise performance of the film makes it highly desirable for the development of sensitive high-T_c bolometers [10] [11] [12]. Immediate applications will be in far infra-red (FIR) instrumentation, operating in the 17 - 250 μm spectral wavelength range, for high-resolution spectroscopy and thermal mapping of cold planetary objects in the solar system. To highlight the need for higher sensitivity bolometers, consider instruments such as the Composite Infra-Red Spectrometer (CIRS) [13] on board the Cassini spacecraft, presently orbiting Saturn and its moons. It has a FIR focal plane that comprises of two single BiTe thermal detectors operating at 170K; each detector with a specific detectivity, D^*, of $\approx 3 \times 10^9$ cm$\sqrt{\text{Hz}}$/W near the low frequency end of a 0.4-to-30 Hz band pass. Observations of the south polar region of Enceladus [14] showed the lack of sensitivity and spatial resolution of the CIRS FIR thermal detectors. However, a focal plane made up of a 2-D array of MgB_2 bolometers, with smaller pixel sizes, higher sensitivity and faster time constant would have enabled higher resolution thermal mapping. Therefore, future planetary missions [15], to the gas giants, icy moons, asteroids and comets, Jupiter and beyond, utilizing remote sensing far-infrared spectroscopic and radiometric instrumentation will greatly benefit from 2-D arrays of thermal detectors with improved D^* and faster τ. Theoretical calculations for an ideal high-T_c bolometer operating at 39K gives a background limited detectivity of

$D^* \approx 3 \times 10^{12}$ cm$\sqrt{\text{Hz}}$/W [16]. However, a practical MgB_2 thin film bolometer using a SiN membrane isolated from the substrate by a weak thermal link, operating at the mid-point of the superconducting transition promises to have a phonon noise limited $D^* \approx 1.6 \times 10^{11}$ cm$\sqrt{\text{Hz}}$/W [11]. Essentially, a constant current biased MgB_2 thin film resistor (thermistor) on a SiN membrane serves as a sensitive thermometer, with a sensitivity defined by the temperature coefficient of resistance at mid-point of transition, $\alpha_m = R_m^{-1}(dR/dT)$, where R_m is the resistance of the thin film at the mid-point of the superconducting transition, T_m. The theory and operation of a high-T_c superconducting bolometer is given elsewhere [17] [18] [19] [20] [21].

If a MgB_2 thin-film bolometer is to be used on future planetary missions, the focal plane assembly will need to be cooled down to 20 K [22], a temperature range not practically attainable with passive radiative coolers. The focal plane will have to be paired with a small mechanical cryocooler with a mass < 1 kg, a power consumption of ≤ 5 W, operating at a reject temperature of ~ 170 K (instrument housing temperature). Even though cryocoolers are now used on missions such as the Hubble Space Telescope and are in development for the James Webb Space Telescope and other missions, there are no space-qualified cryocoolers that presently satisfy the stringent mass and power requirements for outer planet missions. However, substantial efforts are currently underway in both commercial companies, e.g. Sunpower Inc.[1] and Ricor USA Inc.[2] and government agencies, e.g. NASA and DoD, to develop advanced cooling technologies that will meet the requirements to cool MgB_2 bolometer focal plane assemblies and be

[1] http://www.sunpower.com/cryocoolers/cryotel.php

[2] http://www.ricor.com

compatible for use in space. It is therefore desirable that efforts are made at this stage to mature the MgB_2 thin-film bolometer design, fabrication and characterization.

In this paper, we present a design for a MgB_2 thin-film bolometer pixel geometry with constraints on thermal heat capacity, thermal conductance and fabrication processes. A processing procedure for fabricating a 10 x 10 bolometer pixel array is outlined. For one of the arrayed pixels we present results of (i) resistance as a function of temperature, $R(T)$, measurements which establishes the effective thermal conductance, (ii) voltage responsivity as a function of frequency, $\Re_v(f)$, measurements to establish the effective time constant and (iii) noise voltage spectra, $V_n(f)$, measurements near the mid-point of the superconducting transition in order to establish the electrical noise equivalent power, NEP_e, and hence the electrical specific detectivity, D_e^*. The paper then compares the predicted performance of the bolometer tested in this work with state-of-the-art high-T_c bolometers in the literature. This is followed with a discussion on how increasing the absorption efficiency of the pixel and using an encapsulation layer to protect the MgB_2 thin-film from degradation will lead to higher sensitivity bolometers. Finally, the paper concludes with some recommendations for future work.

2. MgB_2 bolometer design

The bolometer design consists essentially of a MgB_2 thin-film resistive meander strongly coupled to an absorber deposited on a thin SiN membrane thermally isolated from a silicon frame using a 4-leg geometry. The incoming radiation, P_{rad} [W], heats up the absorber and changes the electrical resistance, R [Ω], of the thermistor with a temperature coefficient of resistance, $\alpha = (1/R)(dR/dT)$ [K^{-1}]. With a constant current

bias, the voltage across the thermistor changes accordingly and constitutes the output signal that is measured. The membrane, thermistor and absorber with thermal heat capacity, C [J/K], is weakly coupled through a link with a thermal conductance, G [W/K], to the sink temperature, T_0 [K], that gives a first order time constant of $\tau = C/G$ [s]. When the bolometer is used in constant current mode, the electrical resistance change modifies the Joule heating, $P_{bias} = I_{bias}V$ [W], giving rise to an Electro-Thermal Feedback (ETF) [23] [24] into the bolometer that produces an effective thermal conductance, $G_e = G(1 - L_0)$ [W/K], and an effective time constant of $\tau_e = \tau/(1 - L_0)$ [s], where $L_0 = \alpha P_{bias}/G$ is a dimensionless parameter that can be considered as the ETF loop gain. There will be a trade off between high responsivity and faster time constant, but these relationships are a good starting point for establishing the required thermal isolation for the bolometer design. However, several practical considerations place a lower limit on the geometrical size (hence thermal heat capacity), for instance (i) to detect diffraction limited FIR radiation to a cut-off wavelength, $\lambda_c = 250$ μm, will require an absorber area of ≈ 250 μm x 250 μm; (ii) the quality of grain morphology in polycrystalline MgB_2 thin-film will dictate the fidelity of pattern delineation and minimum width resolution in the etching process with regard to both etch selectivity and under etch and (iii) the MgB_2 thin-film resistance needs to be large enough to have good responsivity and also to have ease of electronic readout, i.e., in order to avoid using bulky impedance matched transformers. So the approach taken in this work is to first establish a good estimate of the thermal heat capacity of a practical bolometer that can be fabricated using standard photolithographic processes and then use this value to evaluate the optimal thermal conductance, $G_{opt} = \sqrt{[(\omega C)^2/(\alpha L_0 T_m + (1 - L_0^2))]}$, derived from considering the minimum

NEP, i.e. when $d(NEP)/dG = 0$. Estimations of the total thermal capacity for a 250 μm square pixel size bolometer structure, with and without a gold black absorber are given in Table 1. For a bolometer with the following parameters C = 8 nJ/K, L_0 = 0.3, T_m = 36K, R_m = 1 kΩ, $\omega = 200\pi$, and α = 9 [11] gives a thermal conductance of ≈ 500 nW/K; this value is used for designing the thermal isolation leg geometry, see Table 2.

3. Experiment

3.1 Bolometer Array Fabrication

The starting material for the fabrication process was a silicon-on-insulator 4-inch diameter, 420 μm thick Si <100> handle wafer with the following successive coatings: 250 nm thick thermal oxide layer; 500 nm thick Low Pressure Chemical Vapor Deposition (LPCVD) low stress (100 - 140 MPa) SiN and 300-nm thick MgB_2 film grown by reactive evaporation [2]. The top-level fabrication process entails, (i) photolithography of the MgB_2 layer into arrays of sensor elements, wiring and pads; (ii) photolithography and partially etching the SiN layer into membranes, legs, and dicing streets; (iii) bonding the front side of the wafer to a pyrex wafer using wax; (iv) patterning and removing back side nitride and oxide layers; (v) deep reactive ion etch openings and streets in the silicon substrate down to the front oxide layer; (vi) wet etch the front oxide through the new openings and streets to reveal the nitride membranes and to separate the chips; (vii) laser dicing the bonded wafer; (viii) dry etching of the remaining front nitride and finally releasing the chips in non-aggressive solvent. This fabrication process does not incorporate any encapsulation of the etched MgB_2 pattern and does not include an efficient absorber layer. The processing steps developed to date

gave a pixel yield within a 10 x 10 array of approximately 30%. The above process does not significantly affect the MgB_2 superconducting transition characteristics or introduce a large amount of excess noise [11]. However, given the delicate nature of the processed MgB_2 film, especially to harmful but necessary processing steps that include distilled water, organic solvent rinsing and O_2 plasma cleaning, an encapsulation scheme needs to be developed. The processing yield will significantly increase once this has been addressed. Photographs of the fabricated 10 x 10 MgB_2 thin-film array together with the bolometer pixel tested here are shown in Figure 1.

3.2 $R(T)$, $\Re_v(f)$ and $V_n(f)$ measurements

$R(T)$ transition curves, at current bias levels 1 μA and 5 μA, were obtained using a standard 4-wire resistance method with a programmable current source and a voltage meter under computer control. The array was mounted to a thermal standoff in a light tight liquid He cryostat designed to have a temperature drift < 60μK/s over the temperature range of operation. The bolometer temperature was monitored using a silicon diode (± 0.02 K) configured to a PID temperature controller also under computer control.

The voltage response as a function of frequency, $V_r(f)$, of the bolometer was measured using a 763 K chopped blackbody radiation source. The cryostat dewar is fitted with a warm KRS5 window (0.6 - 60μm) at ≈ 300 K and a cold filter (8.5 - 12.35μm) at ≈ 10 K with transmission efficiencies of 70% and 85% respectively. The geometrical arrangement of blackbody source and transmissive optics gives rise to a $f/\# \approx 23$, with a spot size at the bolometer array plane that substantially overfills the pixel and frame dimensions. Taking into consideration the transmission efficiencies of the window and

cold filter, the total radiation power irradiating the bolometer pixel receiving area is 4.68 nW. The absorption efficiency (emissivity), η, of the bolometer pixel receiving area is calculated from the ratio of electrical to blackbody NEP, i.e. $\eta = NEP_e / NEP_{bb}$, (see §4.2).

For the voltage noise spectra measurements, a battery operated low noise operational amplifier (LNA) and a HP3582A spectrum analyzer were configured to measure the power spectral density of the MgB_2 thin-film thermistor. A 12.5 V battery in series with a wire wound bias resistor (2.5 MΩ) in a shielded box provides the low-noise constant current source. The effect of the bias circuit noise can be ignored when the bias resistor is much larger than the resistance of the bolometer at mid-point [11]. The cryostat dewar, LNA and the bias circuit were housed in a Faraday room to cut down extraneous 60 Hz noise pick-up. The LNA was built around a precision high-speed Difet™ op amp (OPA627)[3] operating in the non-inverting mode. A 0.1 μF capacitor in parallel with a 10 kΩ resistor in the feedback loop limits the bandwidth of the amplifier to ≈ 160 Hz (3dB) and makes its transfer function dominated by a single pole response. The measured amplifier gain within this bandwidth is 101 V/V. A 10 kΩ test resistor at the input termination of the op amp at room temperature gave a noise voltage ≈ 10 nV√Hz, ensuring confidence in the noise measurement test set-up.

3.3 Results

[3] http://www.ti.com/product/opa627

Figure 2 shows $R(T)$ transition curves for bolometer device #E4 operating in the constant current mode for two bias levels 1 μA and 5 μA. The device geometry for this bolometer, pixel design C, is given in Table 2. The effect of Joule heating combined with ETF gives a 0.52 K change at the mid-point of transition. The thermal conductance is numerically calculated for the condition $\int [I_{bias}R/(G - I_{bias}^2 dR/dT)]dI_{bias} = 0.52$, which gives G = 315 nW/K. Figure 3, shows the 5 μA current bias $R(T)$ curve re-plotted for corrected temperature, together with dR/dT calculated from a functional curve fit to the data. The temperature, T_m, and resistance at the mid-point of the transition, R_m, is 36.47 K and 1634 Ω respectively, with a superconducting transition width, ΔT, of 0.35 K determined using the 10% - 90% of R_{40K} rule. The maximum temperature coefficient of resistance is α_{max} = 8.4 K^{-1}, and at mid-point of transition α_{mid} = 5.8 K^{-1}, the residual resistance ratio is, $RRR = R_{300K}/R_{40K} = 1.7$ and the ETF constant is $L_0 = 0.75$ (at α_{mid}). The effective thermal conductance is 79 nW/K and the destabilization current is ≈ 6μA. Figure 4 shows a plot of voltage response, $V_r(f)$ with an amplifier gain of g =101. The effective time constant, τ_{eff}, is determined by fitting the data to the function $V_r = V_0/\sqrt{(1 + (2\pi f\tau_{eff})^2)}$, the curve fit gives V_0 = 53.83 mV and τ_{eff} = 5.2 ms. The low noise amplifier 3dB roll-off at 160Hz is evident. From this, the voltage responsivity as a function of frequency, i.e., $\Re_v(f) = V_r(f)/gP_{rad}$, can be determined, see the inset of Figure 4, and shows a dc voltage responsivity of ≈ 982 kV/W. The measured G and τ, is consistent with the estimated heat capacity, calculated from published specific heat capacity data, for the SiN membrane and MgB_2 thin-film thermistor, i.e., $C = G\tau \approx$ 2nJ/K, see Table 1.

Voltage noise spectra, $V_n(f)$, using a 5 μA current bias, were measured using 64 averages, for several temperatures within the superconducting transition, see Figure 5. The voltage noise spectrum for a resistance $R =$ 1516 Ω (close to the mid-point of transition) is shown in Figure 6, together with the measurement system baseline noise. The system noise baseline is established by measuring the voltage noise spectrum when the MgB_2 thin-film is superconducting. This is equivalent to a shorted input of the noise measurement system but additionally gives the noise contributions of wiring and contact resistances within the cryostat. In Figure 6, the 1516 Ω raw noise spectrum is smoothed with a number of successive median filters to within < 5% error and subjected to gain correction and subtraction in quadrature of the system baseline noise. The noise spikes at 10, 20, 30 and 40 Hz, seen in the data before smoothing, are due to the control current of the PID temperature controller. This was verified by measuring the power spectrum of the temperature controller heater output through a low noise differential amplifier, while controlling the temperature near 36 K.

The electrical NEP, i.e., $NEP_e(f) = V_n(f)/\Re_v(f)$ is shown in Figure 7(a) it assumes 11.6% power absorption efficiency (η) for the pixel area (see §4.2). The NEP_e at 30Hz is 256 fW/√Hz. From this, the blackbody NEP, i.e., $NEP_{bb} = NEP_e/\eta$ can be calculated for more optimized absorbers. The increase in NEP_e centered around 60 Hz is due to extra noise pickup. In Figure 7(b), the electrical detectivity, $D_e^*(f) = \sqrt{A_d}/NEP_e$ is plotted and shows a $D_e^* = 7.6 \times 10^{10}$ cm√Hz/W operating at 30Hz. Table 3 gives the performance of the bolometer tested together with the predicted blackbody D_{bb}^*'s for a bolometer coated with absorption layers with better efficiencies.

4. Discussion

4.1. Comparison with existing high-T_c bolometers

Many groups have worked on thinned substrate/membrane and micromachined silicon based high-T_c bolometers that use cuprate compounds (YBCO, GdBaCuO etc.) as the thermistor material. To the best of our knowledge only Portesi *et al.*, [12] have fabricated a MgB_2 thin-film based bolometer. Based on D^* and τ values reported by these groups the invariant detectivity, a frequency independent parameter, $\Delta = D^*/\sqrt{\tau}$ [cm/J] as a function of τ is plotted in Figure 8, to illustrate the sensitivity versus time constant compromise. The data points (*a*-to-*q*) have been compiled from Khrebtov *et al.*, [21], Verghese *et al.*, [25], Lakew *et al.*, [10] [26] [27], Brasunas *et al.*, [28], Li *et al.*, [29] and Neff *et al.*, [30]. Included on this plot is the invariant electrical detectivity, 1.2 x 10^{11} cm/J for the bolometer characterized in this work. For comparison, using the best D^* reported in the literature [31], the state-of-the-art invariant detectivity, $\Delta = 5.4 \times 10^{10}/\sqrt{\tau}$ cm/J, is also plotted. It can be seen that the MgB_2 thin-film bolometer reported here has more than a magnitude improvement in τ performance when compared to the best D^* previously reported. In order to see what level of sensitivity improvement can be realistically expected, the theoretical upper limits for a bolometer operating at 95K (YBCO) and 39K (MgB_2), i.e., $\Delta = 3.2 \times 10^{11}/\sqrt{\tau}$ and $\Delta = 2.97 \times 10^{12}/\sqrt{\tau}$ respectively, are also plotted and shows that there is still room for marked improvement.

4.2. Influence of pixel absorber

4.2.1 MgB_2-SiN absorber

In Figure 8, the invariant detectivity for the bolometer pixel tested in this work with no efficient absorber is shown. In evaluating this figure-of-merit, the absorption efficiency was calculated, using the relationship $\eta = NEP_e / NEP_{bb}$, to be ≈ 11.6% for a bolometer pixel receiving area of 250 μm x 250 μm in the 8.5 - 12.35 μm spectral radiation band. This value is consistent with the low but different absorption efficiencies of the MgB_2 thin-film resistive meander (≈ 67% of pixel receiving area) and the remaining exposed SiN membrane, see Figure 1. The MgB_2 thin-film in this spectral region has an absorption efficiency of ≈ 14% [32] and the SiN membrane shows a strong broad Si-N absorption feature at 7.87μm [33] [34] with an absorbance between ≈ 3% and 19% within the 8.5 – 12.35 μm band pass [35]. Since the power contribution is not uniform in this bandpass, the weighted average absorbance is calculated for 1μm wavelength steps, this gives a SiN membrane absorbance of 11%. The combined effect of MgB_2 thin-film and SiN membrane absorbance gives the overall weighted average absorption efficiency for the pixel of ≈ 13%.

4.2.2 Influence of cavity underneath pixel

The bolometer array is epoxy bonded onto a gold coated ceramic package; therefore a cavity of ≈ 500 μm (much greater than required for cavity resonance) exists underneath the pixel, comprising the thickness of the silicon frame and the epoxy bond. In the D_e^* evaluation it was assumed that the blackbody radiation not only overfills the pixel area but that it is well collimated so that all the source radiance that enters into the cavity at

normal incidence reflects out and does not irradiate the back of the pixel. Since the gold-coated ceramic is not an ideal mirror then spurious reflections can account for irradiance onto the back of the pixel. In the worst-case scenario i.e., where all the radiation that enters the cavity reflects from the gold coated ceramic at 60% reflection efficiency and irradiates the back of the SiN membrane pixel with a 11% absorption efficiency then a worst-case electrical specific detectivity of 4.2 x 10^{10} cm√Hz/W is evaluated. It is therefore reasonable to report an electrical D_e^* between 4.2-to-7.6 x 10^{10} cm√Hz/W operating at 30Hz for the bolometer characterized in this work.

4.2.3 Space matched and gold black absorber

If a space matched bismuth coating with a sheet resistance of 188 Ω/square (50% absorption in all wavelengths up to 250μm) is deposited on the pixel receiving area then the measured optical detectivity, $D_{bb}^* = 8.8 \times 10^9$ cm√Hz/W is predicted to improve to ≈ 3.8 x 10^{10} cm√Hz/W, however the time constant of the bolometer will increase from ≈ 5 ms to ≈ 14.5 ms due to the extra thermal heat capacity of the Bi absorber, see Table 1. However, for the same pixel receiving area, if a 12 μm thick gold black coating with a material density of 174 Kg/m^3 is deposited that has ≈ 85% absorption efficiency in the 20 – 250 μm spectral band [36] then the optical detectivity is predicted to improve further to ≈ 6.4 x 10^{10} cm√Hz/W with a time constant of ≈ 18 ms, again due to the increase in thermal mass, see Table 1. Figure 8 shows the predicted D_{bb}^* and τ values for the bismuth and gold black coating i.e., Δ ≈ 3.1 x 10^{11} cm/J and ≈ 4.8 x 10^{11} cm/J respectively, for comparison the theoretical Δ for a 39K thermal detector operating at ≈ 10 Hz is 2.2 x 10^{13} cm/J and highlights that a gold black coated bolometer like the one

constructed in this work is a factor of ≈ 46 away from what is theoretically possible and ≈ 2.5 from the findings of a previous paper [11] where it was predicted that an optimized phonon noise limited bolometer with a $D^*_{bb} = 1.6 \times 10^{11}$ cm√Hz/W operating at 30Hz could be realized based on $1/f$ (excess) noise measurement of an etched MgB_2 thin-film resistor.

4.4. MgB_2 thin-film aging

The bolometer device pixel was characterized approximately 2-years after the bolometer array was fabricated. Although the bolometer array was stored under a soft vacuum, the room temperature MgB_2 thin film meander resistance increased from 3500 Ω to 5200 Ω, a ≈ 1.5 fold increase. The superconducting transition properties also changed with aging, ΔT increased from 0.2 K to 0.35 K, T_{mid} decreased from 37.12 K to 36.47 K and R_m increased from 1000 Ω to 1634 Ω. It is unclear whether the increase in the electrical resistance at the mid-point of the superconducting transition is also indicative of an increase in the thermal impedance of the film, a key parameter in evaluating the optimal thermal conductance for the bolometer design (see §4.5). A necessary requirement for future bolometer arrays for FIR instrumentation will be to ensure that the MgB_2 thin-film thermistors are robust in air at atmospheric pressure during the integration cycle; it is therefore essential that a good passivation scheme be developed. The results of the aging study will be reported in a future paper.

4.5 Optimal thermal conductance

The thermal conductance, 315 nW/K, from $R(T)$ measurements is significantly smaller than the optimal design value of ≈ 500 nW/K arrived at using estimated parameters (see §2). If the measured parameters, L_0 = 0.75, and α = 5.8 are used, with all other parameters remaining the same, then $G_{opt} \approx$ 400 nW/K. Also, for the optimal design value of 500 nW/K the isolation leg geometry was designed using a MgB_2 thin film thermal conductivity of 7 W/m/K, an average value established from two works in the literature, see Table 2. The measured thermal conductance of 315 nW/K and the recalculated value of 400 nW/K would indicate that the MgB_2 thin film thermal conductivity is between 3-to-5 W/m/K at 36K, a value more consistent with the findings of Podder *et al.* [37].

4.6 Future work

At this stage of development, improvements will focus on (i) refining the photolithographic processes in order to fabricate a second generation bolometer array with higher pixel yield; (ii) developing a reliable and robust passivation layer that fully encapsulates the MgB_2 thin-film meander, including the sidewalls and also to ensure that the passivation layer has good adhesion to the SiN membrane; (iii) investigating whether a thinner MgB_2 film, with the same or superior superconducting properties, can be used in order to reduce thermal heat capacity; (iv) developing an efficient absorber layer with minimum heat capacity in order to improve the time constant and (v) integrating a Winston cone concentrator in front of a bolometer pixel and repeating the characterization. Future work also includes radiometric characterization of bolometer

pixels with different leg geometries in order to further understand the MgB_2 film/SiN thermal conductance so that models can be improved in order to design and fabricate bolometers with better performance.

5. Summary

A SiN membrane based MgB_2 thin-film bolometer, with a non-optimized radiation absorber, has been designed, fabricated and tested that shows a D_e^* = 4.2-to-7.6 x 10^{10} cm√Hz/W operating at 30Hz. in the 8.5 - 12.35 μm spectral band. It has also been shown, that with the integration of a gold black coating on a bolometer such as the one constructed in this work, a blackbody specific detectivity of D_{bb}^* = 6.4 x 10^{10} cm√Hz/W at an operational frequency of 10Hz can be realized for integration into future planetary exploration instrumentation where high sensitivity is required in the 17 - 250 μm wavelength spectral range.

Figure 1. (a) Photograph of a packaged (10 x 10) MgB_2 bolometer array and (b) MgB_2 bolometer pixel showing the resistive meander, see pixel C in Table 2 for dimensions.

(a)

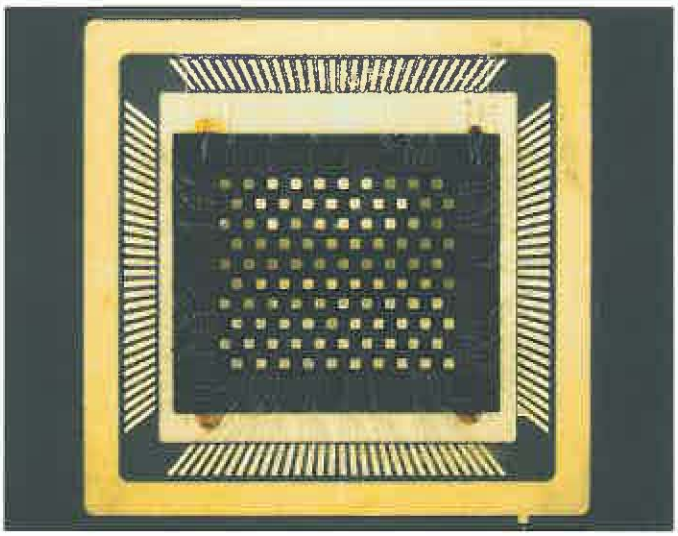

(b)

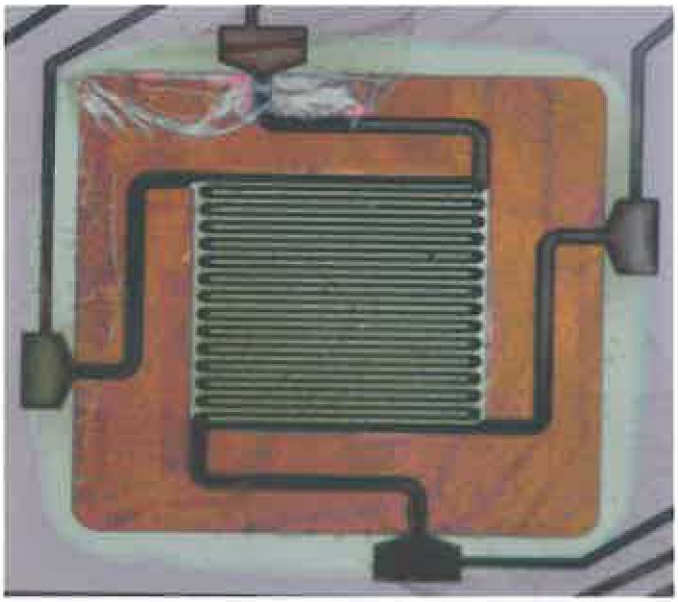

Figure 2. $R(T)$ for I_{bias} =1 μA and 5 μA. The thermal conductance is calculated at the mid-point of transition by numerical integration.

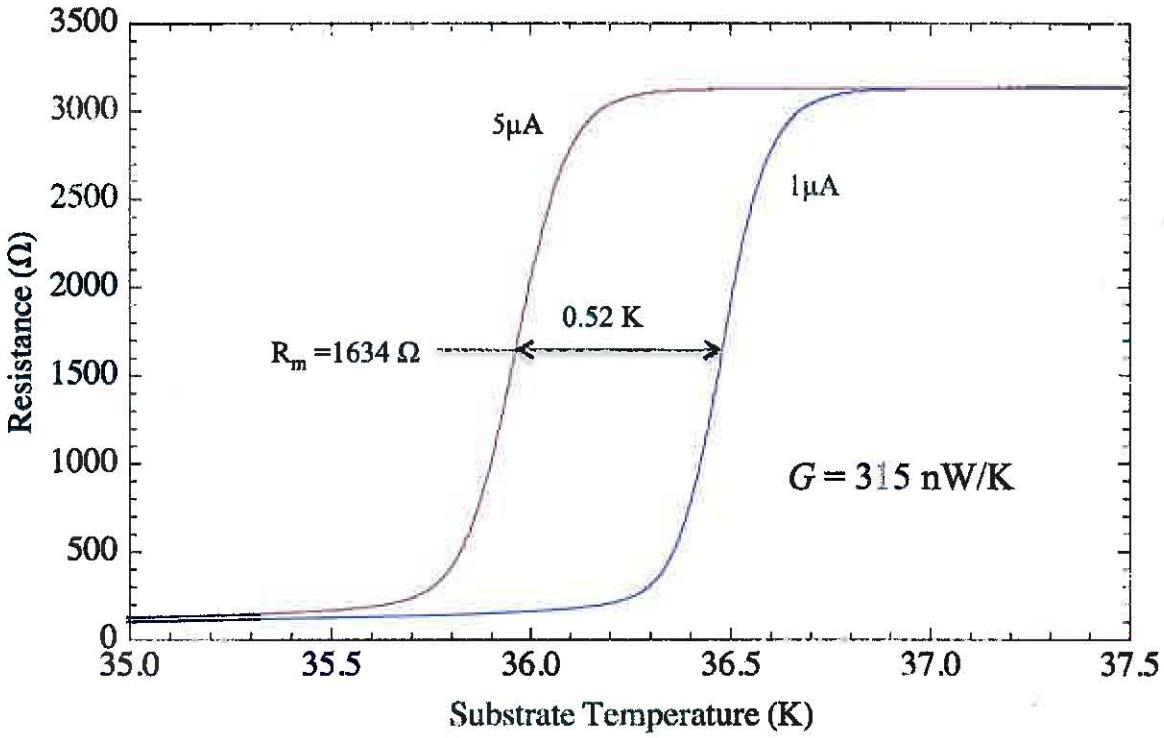

Figure 3. R, dR/dT and α as a function of corrected substrate temperature.

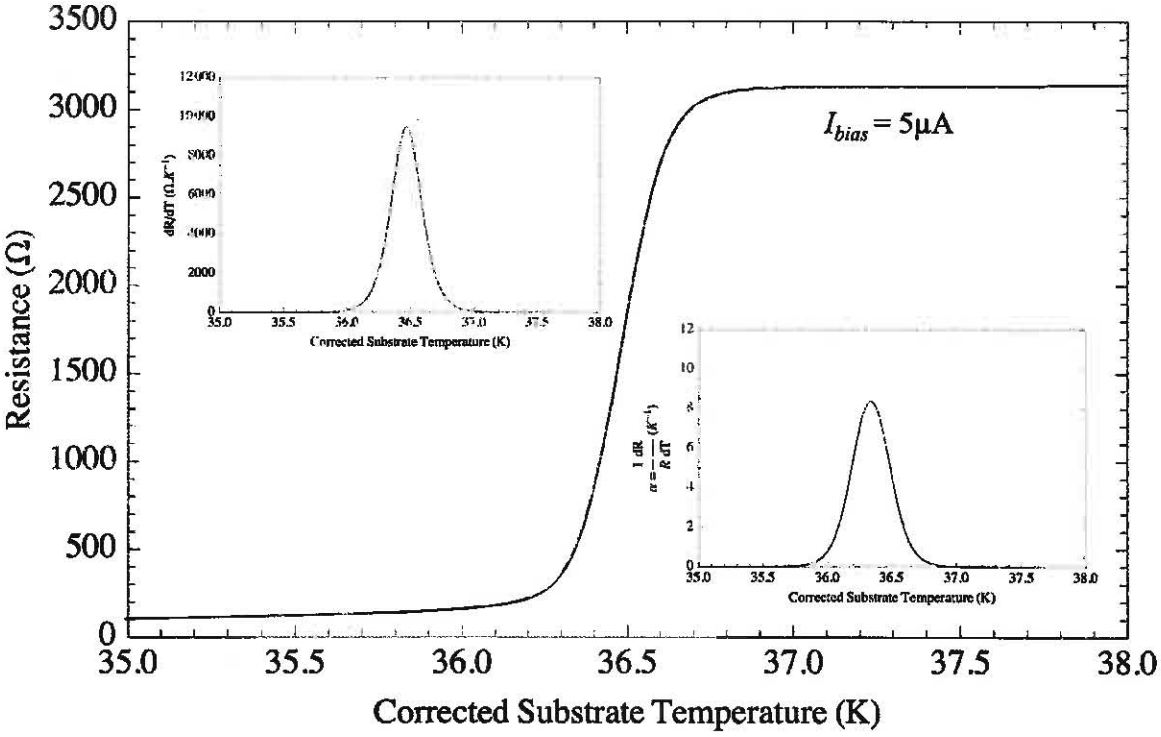

Figure 4. Voltage response (with $g = 101$) and reponsivity (inset), after gain correction, of the bolometer to a chopped 763 K blackbody source. The responsivity is 701 kV/W at 30Hz. The 3dB roll-off for the op-amp is at 160Hz.

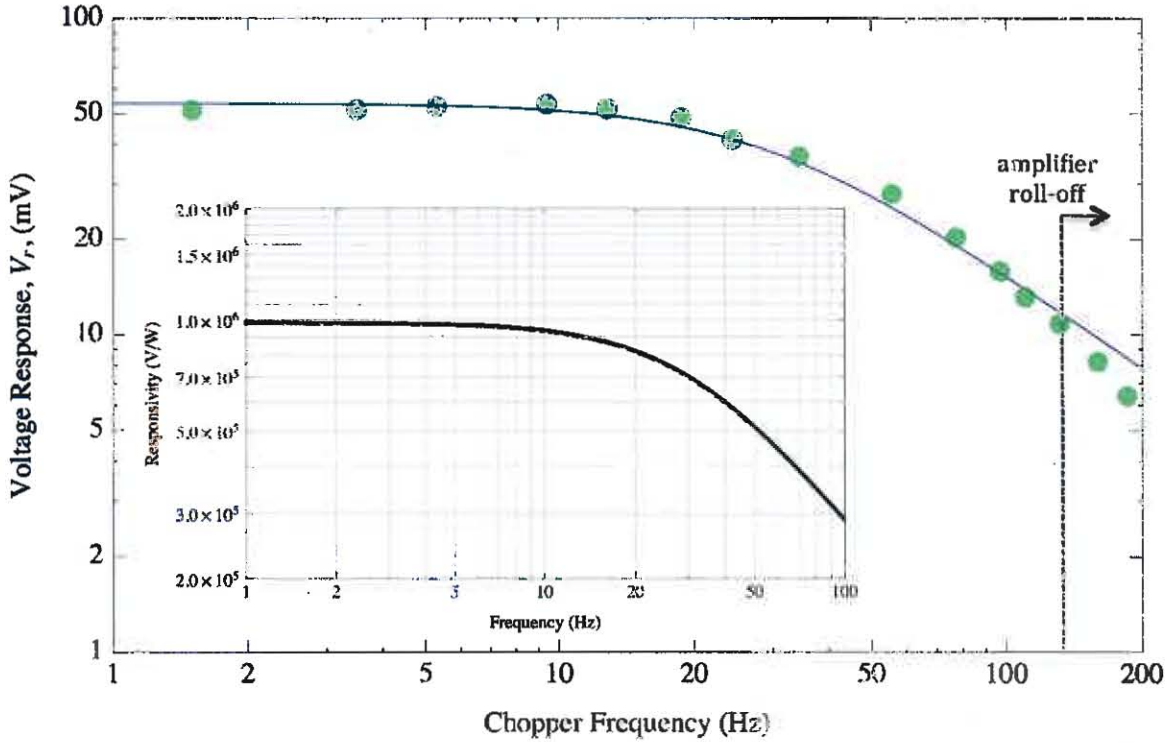

Figure 5. Voltage noise spectra averaged over 64 samples, corrected for system baseline noise and gain, for various resistances within the superconducting transition.

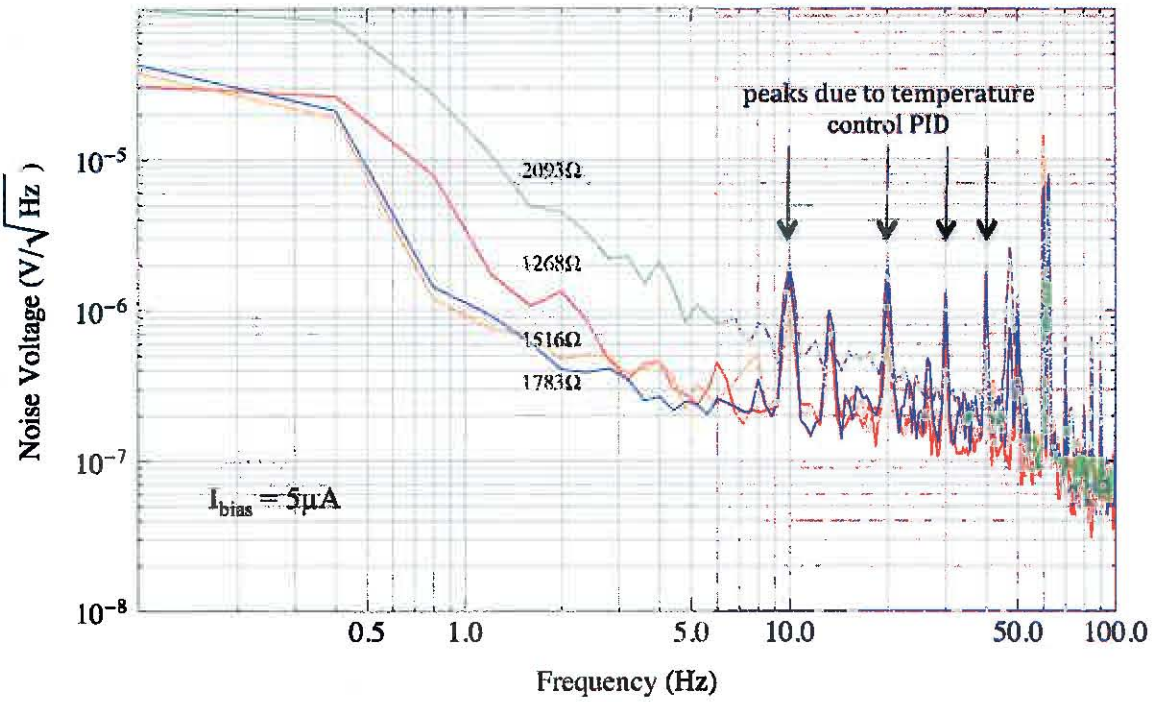

Figure 6. Voltage noise spectra for 1516 Ω resistance, with a current bias of 5μA, near the mid-point of the superconducting transition. The system noise floor is also shown.

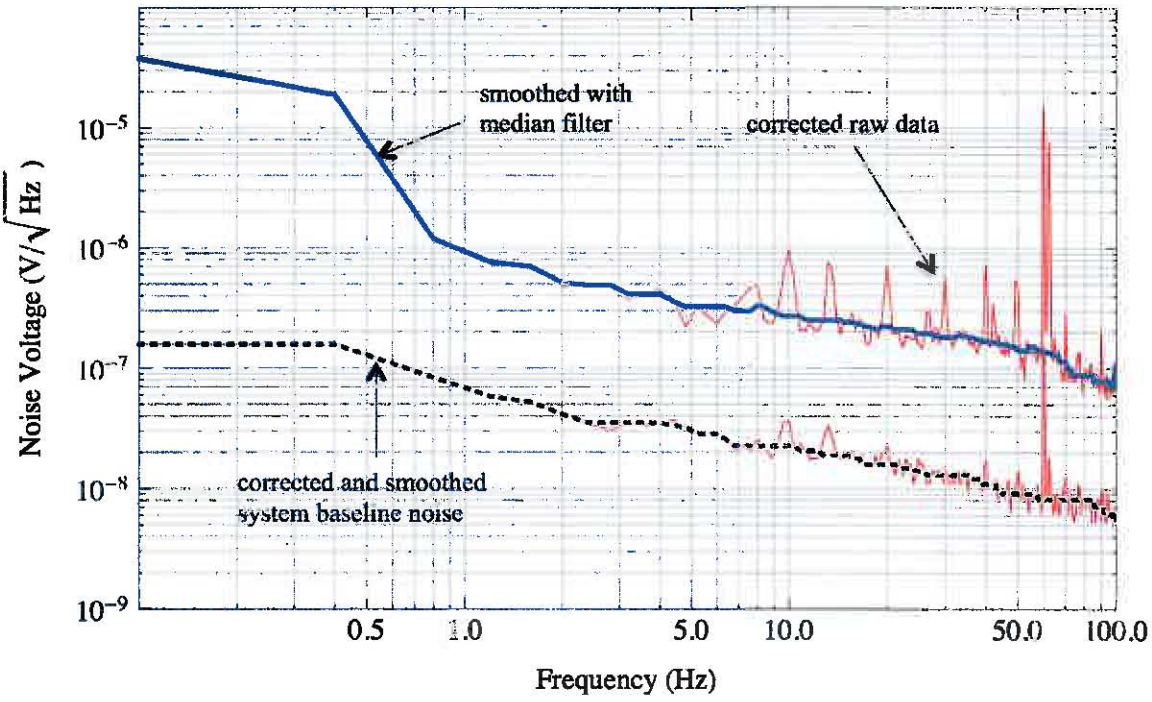

Figure 7. (a) NEP_e and (b) D_e^* as a function of frequency.

(a)

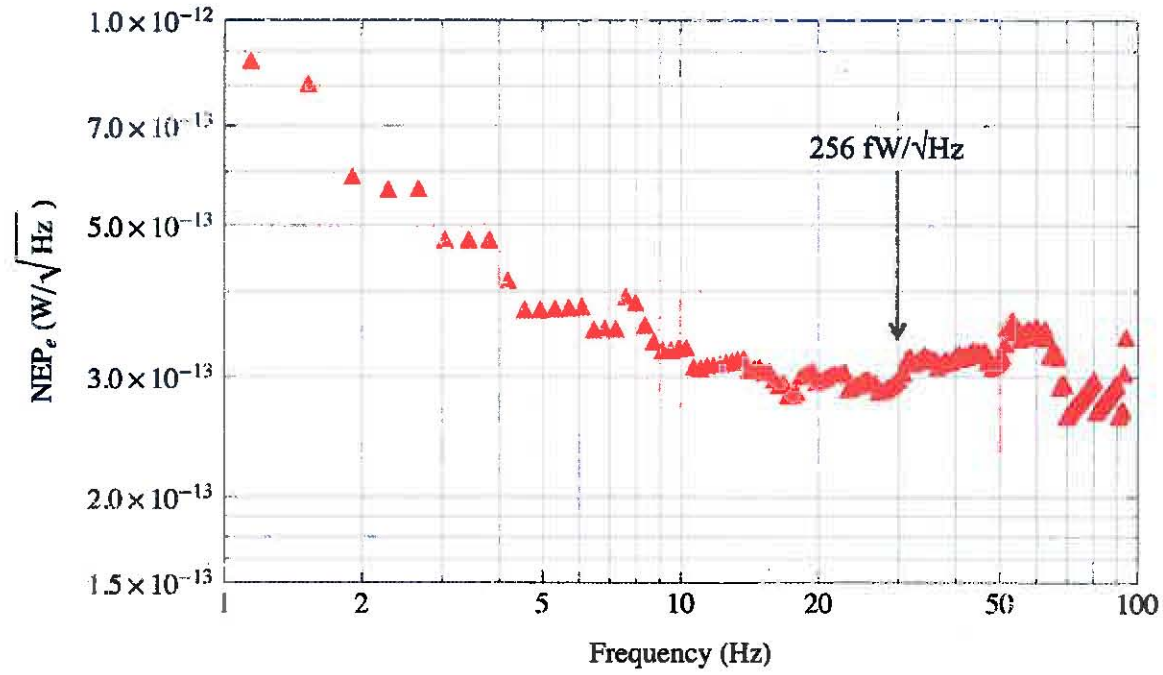

(b)

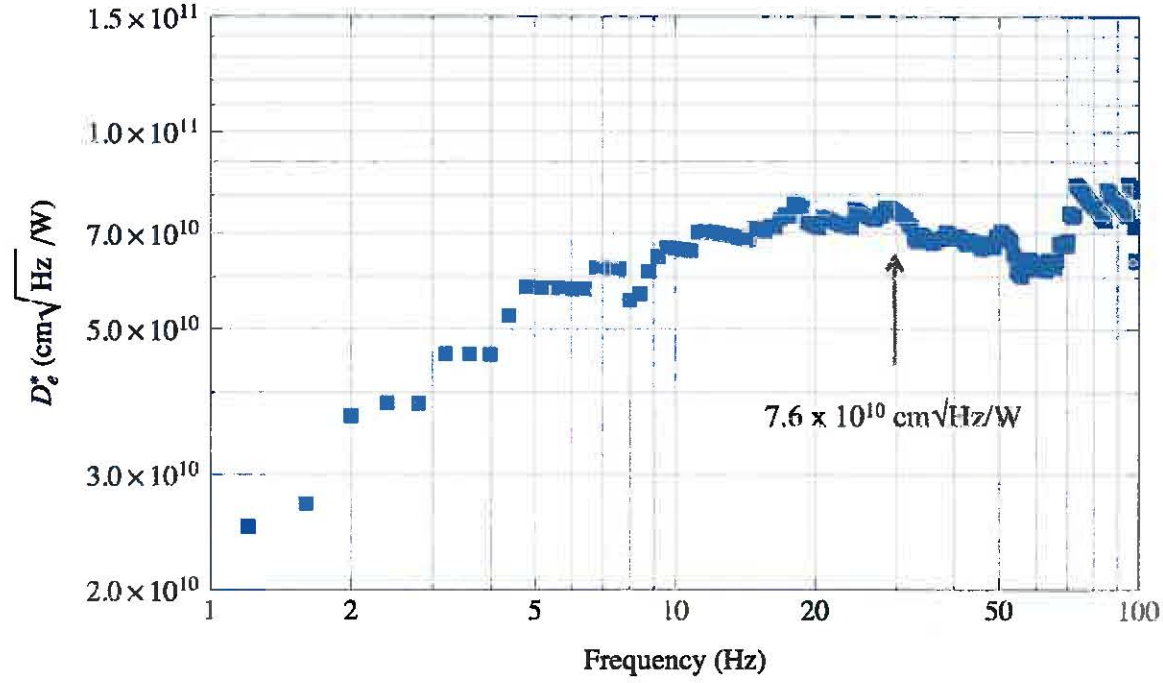

Figure 8. The invariant detectivity, $D^*/\sqrt{\tau}$, as a function of time constant, τ, for the bolometer fabricated in this work compared to state-of-the-art thinned substrate and monolithic silicon based high-T_c bolometers reported in the literature.

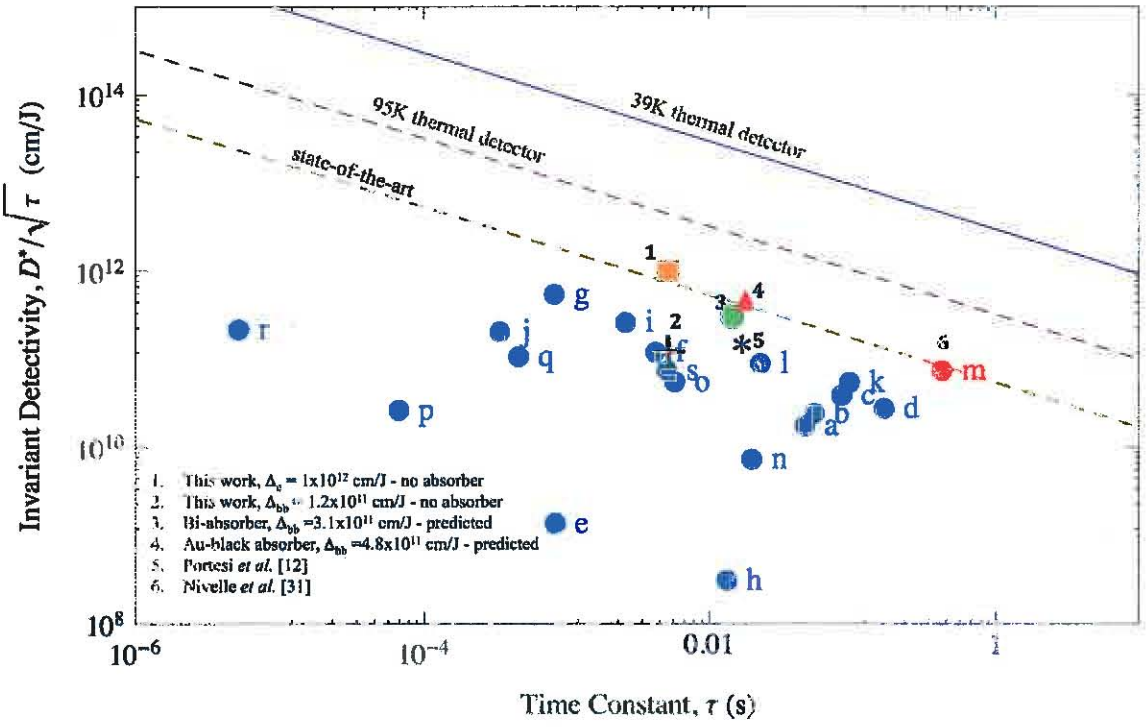

Table 1. Physical properties of bolometer material layers at 35K.

Layer	Specific heat capacity s (J/Kg/K)	Thermal conductivity k (W/mK)	Density ρ (Kg/m^3)	Area A (10^{-9} m^2)	Thickness t (μm)	Heat capacity C (nJ/K)
SiN-membrane[a]	20	1.5	2900	63.9	0.5	1.83
MgB_2 film[b]	13.6	5, 9[d]	2570	44.65	0.3	0.36
Bi-absorber[c]	63.29	-	9800	62.5	0.1	3.88
Au-black absorber	42	-	173.5	62.5	12	5.47
C without absorber*	-	-	-	-	-	2.19
Total C with Bi*	-	-	-	-	-	6.07
Total C with Au-black*						7.66

[a] [38] [39]; [b] [40] [37]; [c] [41]; [d] [42]; *add extra 6% if full legs are taken into consideration

Table 2. MgB_2 bolometer pixel and isolation leg geometry. Thermal conductance calculation based on SiN and MgB_2 thin film thermal conductivity of 1.5 W/m/K and 7 W/m/K respectively.

Pixel design	Membrane size (μm^2)	SiN leg length (μm)	SiN leg width (μm)	MgB_2 leg width (μm)	Thermal conductance (nW/K)
A	250 x 250	150	10	5	478
B	250 x 250	200	10	5	359
C	250 x 250	250	14	10	503
D	250 x 250	350	14	10	359

Pixel C and was used in this testing

Table 3. Summary of MgB_2 bolometer characterization

Parameter	Value	Comments
Bias Current	5 μA	Constant current mode
Transition width	0.35K	10% - 90% of R_{40K}
Mid-point of transition	1634 Ω	-
Temperature coefficient of resistance	5.8 K^{-1}	@ mid-point
RRR	1.7	R_{300K}/R_{40K}
ETF constant	0.75	-
Thermal conductance	315 nW/K	-
Effective first-order time constant	5.2 ms	-
Pixel absorption efficiency	11.6 %	See section §4.2
Voltage responsivity	701 kV/W	@ 30Hz
Equivalent noise bandwidth	0.6 Hz	-
Electrical NEP_e	256 fW/√Hz	@ 30Hz
Best case electrical D^* (no absorber)	7.6×10^{10} cm/√Hz/W	@ 30Hz
Worst case electrical D^* (no absorber)	4.2×10^{10} cm√Hz/W	@ 30Hz
Best case blackbody D^* (no absorber)	8.8×10^{9} cm√Hz/W	@ 10Hz
Worst case blackbody D^* (no absorber)	3.8×10^{9} cm√Hz/W	@ 10Hz
Predicted blackbody D^* (Bi-absorber)	3.8×10^{10} cm√Hz/W	@ 10Hz
Predicted blackbody D* (Au-black absorber)	6.4×10^{10} cm√Hz/W	@ 10Hz

Acknowledgements:

The authors wish to thank Dr. Simon Bandler (University of Maryland) for enlightening conversations regarding ac impedance measurements on superconducting films. This work was supported by Goddard Space Flight Center IRAD funding.

References

[1] J. Nagamatsu, N. Nakgawa, T. Muranaka, Y. Zenitani, and J. Akimitsu, "Superconductivity at 39K in magnesium diboride," *Nature*, vol. 410, pp. 63-64, 2001.

[2] Michio Naito and Kenji Ueda, "MgB2 thin films for superconducting electronics," *Superconductor Science and Technology*, vol. 17, pp. R1-R18, 2004.

[3] S. Bevilacqua et al., "Low noise MgB2 terahertz hot-electron bolometer mixers," *Applied Physics Letters*, vol. 100, no. 3, pp. 033504-033504-3, January 2012.

[4] H. Shimakage and Z Wang, "MgB2 thin films amd MgB2/AlN/MgB2 SIS jinctions," *Physica C*, vol. 435, pp. 66-70, February 2006.

[5] S. Miki et al., "Nanofabrication of superconducting MgB2 neutron detector," *Nuclear Instruments and methods in Physics Research A*, vol. 529, pp. 405-408, 2004.

[6] H. Yamamoto and et al., "Fabrication and characterization of resonant devices using superconducting MgB2 thin films," *Physica C*, vol. 463-465, pp. 948-951, 2007.

[7] B. H. Moeckley, K. E. Kihlstrom, A. T. Findikoglu, and D. E. Oates, "Microwave properties of MgB2 thin fils by reactive evaporation," *IEEE Trans. on Appl. Supercond.*, vol. 15, pp. 3308-3312, 2005.

[8] X. X. Xi, "MgB2 thin films," *Supercond. Sci. Technol.*, vol. 22, no. 4, p. 043001, 2009.

[9] E. Monticone, M. Rajteri, C. Portesi, S. Bodoardo, and R. S. Gonnelli, "MgB2 superconducting films for bolometer applications," *IEEE Transactions on Applied Superconductivity*, vol. 13, no. 2, 2003.

[10] B. Lakew et al., "Effect of ionizing radiation on noise in MgB2 thin film - a candidate material for detector development for post-Cassini planetary missions," *Physica C*, vol. 440, pp. 1-5, 2006.

[11] B. Lakew, S. Aslam, H. Jones, T. Stevenson, and N. Cao, "1/f noise in the superconducting transition of a MgB2 thin film," *Physica C*, 2010.

[12] C. Portesi, E. Taralli, R. Introzzi, M. Rajteri, and E. Monticone, "Fabrication and characterisation of an MgB2 bolometer," *Supercond. Sci. Technol*, vol. 20, pp. S403-S407, 2007.

[13] V Kunde, "SPIE Proceedings," , vol. 2803, 1996, p. 162.

[14] J. R. Spencer et al., "Cassini Encounters Enceladus: Background and the Discovery of a South Polar Hot Spot," *Science*, vol. 311, no. 5766, pp. 1401-1405.

[15] "Vision and Voyages for Planetary Science Decade 2013-2022," NRC of the National Academies, 100309209544, 2011.

[16] R. A. Smith, F. E. Jones, and R. P. Chasmar, *The detection and measurement of infra-red radiation.*: Oxford University Press, 1968.

[17] P. W. Kruse, "Physics and applications of high-Tc superconductors for infrared detectors," *Semicond. Sci. Technol.* , vol. 5, no. S229, 1990.

[18] P. L. Richards, "Bolometers for Infrared and millimeter waves," *J. Appl. Phys.*, vol. 76, p. 1, 1994.

[19] P. L. Richards et al., "Feasability of the high-Tc superconducting bolometer," *Appl. Phys. Lett.*, vol. 54, pp. 283-285, 1989.

[20] M., Torrence Walcott, *Bolometers Theory, Types and Applications*, 1st ed., Torrence M. Walcott, Ed. New York, USA: Nova Science Publishers, Inc., 2009.

[21] I., A. Khrebtov and A. D. Tkachenko, "High-temperature superconducting bolometers based on silicon-membrane technology," *J. Opt. Technol.*, vol. 71, no. 3, pp. 143-152, 2004.

[22] A., Paul Richards, "Superconducting TES Bolometers above 1K," in *TDW'03, International Thermal Detectors Workshop*, 2003, pp. 2-1.

[23] J. Mather, *Appl. Opt.*, vol. 21, p. 1125, 1982.

[24] K. Irwin, "Appl. Phys. Lett.," vol. 66, p. 1998, 1995.

[25] Verghese et al., "IEEE Trans. Appl. Supercond.," vol. 3, p. 2115, 1993.

[26] Lakew B. et. al., *Physica C*, vol. 329, pp. 69-74, 2000.

[27] Lakew B. et al., *Sensors and Actuators A*, vol. 114, pp. 36-40, 2004.

[28] J. Brasunas and B. Lakew, *Appl. Phys. Lett.*, vol. 64, p. 777, 1994.

[29] H. et al. Li, *IEEE Trans. Appl. Supercond,* vol. 7, p. 2371, 1997.

[30] Neff H. et al., *Appl. Phys. Lett.*, vol. 67, p. 1917, 1995.

[31] M. J. M. E. Nivelle, *IEEE Trans. Appl. Supercond.*, vol. 9, p. 3350, 1999.

[32] J. J. Tu et al., "Optical properties of c-axis oriented superconducting MgB2 films,"

Physical Review Letters, vol. 87, no. 27, pp. 277001-1-277001-4, 2001.

[33] G. Santana and A. Morales-Acevedo, "Optimization of PECVD SiN:H films for silicon solar cells," *Solar Energy Materials & Solar Cells*, vol. 60, pp. 135-142, 2000.

[34] W. R. Knolle and D. L. Allara, "Infrared spectroscopic characterization of silicon nitride films - optical dispersion induced frequency shifts," *Applied Spectroscopy*, vol. 40, no. 7, pp. 1046-1049, 1986.

[35] M. Molinari and H., Vergnat, M. Rinnert, "Preperation of dense smooth and homogeneous amorphous silicon nitride films by nitrogen-ion-beam assissted evaporation," *J. Phys. D: Appl. Phys.*, no. 41, p. 175410 4pp, 2008.

[36] W. Becker, R. Fettig, A. Gaymann, and W. Ruppel, "Black gold deposits as absorbers for far infrared radiation," *Phys. stat. sol. (b)*, vol. 194, p. 241, 1996.

[37] Podder, *Physica C*, vol. 390, p. 191, 2003.

[38] B. L. Zink and F. Hellman, "Specific haet and thermal conductivity of low-stress amorphous Si-N membranes," *Solid State Communications*, vol. 129, 2004.

[39] Holmes, *Appl. Phys. Lett.*, vol. 72, p. 2250, 1998.

[40] R. K. Kremer, B. J. Gibson, and K. Ahn, "Heat capcity of MgB2: Evidence for moderately strong coupling behavior".

[41] T. C. Cetas, J. C. Holste, and C. A. Swenson, "Heat Capacities from 1 to 30K of Zn, Cd, Sn, Bi, and Y," *Physical Review*, vol. 182, no. 3, pp. 679-685, June 1969.

[42] T. Muranaka, J. Akimitsu, and M. Sera, "Thermal transport properties of MgB2," *Physical Review B*, vol. 64, pp. 020505-1-020505-3, June 2001.